minerals

MDPI

Article

Rare Earth Element (REE) and Critical Mineral Fractions of Central Appalachian Coal-Related Strata Determined by 7-Step Sequential Extraction

Sophia Bauer [1,2,*], Jonathan Yang [1,2], Mengling Stuckman [3,4] and Circe Verba [1]

[1] National Energy Technology Laboratory, Albany, OR 97321, USA
[2] NETL Support Contractor, Albany, OR 97321, USA
[3] National Energy Technology Laboratory, Pittsburgh, PA 15236, USA
[4] NETL Support Contractor, Pittsburgh, PA 15236, USA
* Correspondence: sophia.bauer@netl.doe.gov

Abstract: Rare earth elements (REEs) and critical minerals (CMs) are used in many modern industries, including the automotive sector, generation and storage, clean energy, and defense. The demand for REEs is increasing, and the REE supply chain is unpredictable. The US has driven to assess non-conventional sources of REE (such as coal underclay) to identify domestic resources to stabilize this uncertainty in supply. Knowledge of the minerology, distribution, and modes of occurrence of REEs is integral to the assessment of non-conventional sources. Additionally, extraction techniques can be optimized and targeted when REE distribution in different solid fractions from source material is understood. In this study, four bituminous coal-related samples associated with the Lower and Middle Kittanning coal seams in the Appalachian Basin (US) underwent a seven-step sequential extraction procedure, primarily targeting the water-soluble, exchangeable, acid soluble, mildly reducible, moderately reducible, strongly reducible, and oxidizable fractions. The REE and other elements of interest from each extraction step were analyzed, and the percentages of element extracted from raw solids were calculated. REEs extracted from the total seven steps were reported as the extractable fraction, whereas the fractions in the residual solids were reported as the non-extractable fraction. Less than 6% of REE were extracted from three samples. Twenty-one percent of REE was extracted from the fourth sample, mainly from the steps targeting oxidizable and exchangeable phases. Co-extraction of critical metals (Co, Ni, Cu, and Zn) occurred during the oxidizable, exchangeable, acid soluble, and water-soluble steps for the four samples. In the extracted fractions, the four samples all exhibited a middle and heavy REE enrichment relative to light REE. The mobility of major cation (e.g., Ca, Fe, and P) and REE is associated with exchangeable, oxidizable, and acid soluble fractions. Non-extractable REE is likely held in refractory apatitic phases, and/or primary REE-phosphates (e.g., monazite and xenotime).

Keywords: rare earth elements; critical minerals; coal underclay

Citation: Bauer, S.; Yang, J.; Stuckman, M.; Verba, C. Rare Earth Element (REE) and Critical Mineral Fractions of Central Appalachian Coal-Related Strata Determined by 7-Step Sequential Extraction. *Minerals* **2022**, *12*, 1350. https://doi.org/10.3390/min12111350

Academic Editor: Rajesh Kumar Jyothi

Received: 2 September 2022
Accepted: 20 October 2022
Published: 25 October 2022

1. Introduction

Rare earth elements (REEs) are a group of elements including the 14 naturally occurring lanthanide elements as well as yttrium (Y) and scandium (Sc). REEs play a critical role in modern technologies and are integral in many aspects of the day-to-day lives of people across the globe. The increased utilization of REE in past decades spans various sectors including but not limited to the defense sector, the energy sector, and the automotive sector [1]. Additionally, there has been an increase in demand for other critical metals (e.g., Co, Ni, Cu, and Zn) that are critical for US economic growth and national security [2]. Overarching many of these sectors is the push for a greener economy [1,3]. REEs play an integral role in novel industrial advancements for green technologies. With the increased demand

for REEs (especially heavy REEs) in multiple sectors, investigation into unconventional source materials can help expand the resources used to obtain REEs [1,3].

Although the REEs are commonly found distributed across the Earth's crust, the concentrations are generally too low for economically feasible ore mining [4]. The geological strata in which REE can be found include laterites, aluminosilicate-rich clays, and hard rock mineral deposits containing carbonatites and bastnaesite [1,4–6]. Rare-earth-containing deposits have been detected in approximately 34 countries, with the largest estimated rare earth reserve being located within China (42.3% of the world's rare earth reserve) [7]. Carbonatite deposits frequently are enriched in light-atomic-weight REEs (LREEs: La, Ce, Pr, Nd, Sm) and are the main type of deposit where REEs are found [6]. Middle REEs (MREEs: Eu, Gd, Tb, and Dy) have been found in black and gray phosphatic shales [8]. Heavy REEs (HREEs: Y, Ho, Er, Tm, Yb, and Lu) have been found to be in alkaline igneous rocks as well as enriched in ion-adsorbed clays [9,10]. Spanning numerous environments, REE mined globally are mainly found in the minerals such as loparite ($(Ce,Na,Ca)_2(Ti,Nb)_2O_6$), bastnasite ($(Ce,La)(CO_3)F$), monazite ($(La,Ce)PO_4$), as well as in lateritic ion-adsorbed clays [11]. Domestic coal fly ash from the Appalachian Basin has been shown to contain the highest concentrations of REEs, followed by coal fly ash from the Illinois Basin and then coal fly ash from the Powder River Basin [12]. Other alternate, lower-grade resources of REEs could be aluminosilicate-rich clays occurring in layers below coal deposits (i.e., coal underclay), which present ample reactive surfaces to collect mobilized metals during alteration processes such as fluid infiltration [5].

These coal underclays are a potential REE resource because they present a readily available and easily accessible material. There is an estimated 2 billion cubic yards of coal refuse in Pennsylvania, 10 million tons in Virginia, and 120 tons from 21 other coal-producing states that could be readily available as an active feedstock for REE extraction [2,13,14]. Stratigraphic column and cross-section of the Appalachian Basin Middle Pennsylvanian series, including the Lower Kittanning and Middle Kittanning coal zones, as well as Lower Kittanning and Middle Kittanning underclay, is seen in Bauer et al., 2021 [2]. Several studies have characterized and examined the extractability of aluminosilicate-rich underclays or coal refuse-based byproducts [5,15,16]. Apatitic phases of REE, REE oxides/oxyhydroxides, and REE–phosphates can accrue in coal underclays during the weathering of REE-bearing alkaline igneous formations [17]. These REE-rich underclays may become potential REE mining sources due to the higher mobility of REE from redistribution of REE during the weathering of REE-rich host rocks. The multimodal characterization completed by Yang et al. [5] illustrates variability of phosphate phases (e.g., monazite, xenotime, rhabdophane, churchite, and crandallite) as well as the co-localization of LREE with Ca, P, and Ba and HREE with Fe and S across six Central Appalachian coal underclays [5].

The REE association with different mineral fractions within specific domestic coal seam underclays is largely unknown, partly due to variability across coal seam environments and the limited available literature. We can draw upon similarities of REE hosting phases in laterites, as both laterites and coal underclay can have depositional environments with a soil layer rich in Fe-O and alumina with heavily weathered parent rocks, such as clays or igneous rocks, which require cycling of wet–dry seasons. Previously, it has been estimated by the combination of mass balance calculations, sequential extractions, and microscopic evidence that approximately 25% of REE in laterites are held in phosphates [18]. In addition to authigenic REE-bearing phosphate minerals, REE are known to be held by Fe/Mn-oxyhydroxides in laterites [18,19]. The distribution of REEs in laterites, as well as coal underclay in any fraction, will vary due to the heterogeneity of minerology and accumulation history. The goal of this study was to determine REE distribution in four Appalachian Basin samples related to the Lower Kittanning (LKT) and Middle Kittanning (MKT) coal seams to understand the modes of occurrence of these metals. Specifically, this includes determining distribution of REEs throughout the feedstock source, the mode of occurrence of REEs bound to numerous fractions, the heterogeneity between different underclays, and the spatial heterogeneity within a specific type of underclay. The sequen-

tial extraction method used in this study is based on Lin et al. (2018) [20] and Ruttenberg (1992) [21], as seen in Section 2.3. Heavy metal distribution and bioavailability are connected to the physiochemical properties of the substance in which the metals reside [22,23]. In sequential extractions, various reagents can be utilized to extract metal fractions from high mobility to low mobility based on the reagent's selectivity and capacity of extraction [24]. This knowledge will provide additional information to further understand the ways in which the extraction of REEs from coal underclays can be cost efficient and which types of lixiviants will be most efficient at extraction.

2. Materials and Methods

2.1. Feedstock Study Units

Four bituminous coal-related samples were collected from two mines currently producing coal in West Virginia (WV) and Central Pennsylvania (PA) (Table 1). These four coal-related samples are representative samples from current mining, focusing on the LKT coal seam and MKT coal seam, with the samples having similar lithology. The WV MKT underclay and coarse coal refuse were sampled from an underground mine wall and refuse pile, while the Central PA LKT underclay and MKT underclay were sampled from a surface pit mine in Central PA. All four samples were crushed and ground to pass through a 100-mesh (148 μm) sieve.

Table 1. Sample designations with general location and associated coal seam.

Sample Designation	Associated Coal Seam	Location
WV MKT underclay	Middle Kittanning	Taylor Co., WV
WV MKT coarse coal refuse	Middle Kittanning	Taylor Co., WV
Central PA LKT underclay	Lower Kittanning	Clearfield Co., PA
Central PA MKT underclay	Middle Kittanning	Clearfield Co., PA

2.2. X-ray Diffraction (XRD) and Electron Microscopy

Bulk mineralogy was measured on a Rigaku III Ultima diffractometer equipped with a Cu anode (40 kV, 44 mA utilizing Cu radiation over a range of 4.0 to 70 degrees (2-theta) in step sizes of 0.02 degrees and scan times of 2.4 s/step). Whole pattern fitting was conducted in the MDI Jade 9 software to identify mineral phases present.

To better understand the trace mineralogy of the samples, electron microscopy was conducted. All samples were mounted in 1-inch epoxy pucks, polished (steps through 150–1200 grade, followed by diamond slurry of 9 m–1 μm), ultrasonically cleaned, and evaporatively coated with approximately 10 nm of carbon. Backscattered and secondary electron images were collected by a FEI Inspect-F field-emission scanning electron microscope (FE-SEM) and equipped with an Oxford Instruments Energy Dispersive X-ray spectrometer (EDS). The elemental composition was also collected by using a JEOL 8530F Plus Hyper Probe electron probe microanalysis system (EPMA) wavelength dispersive spectroscopy (WDS). SEM and EPMA operating conditions had an accelerating voltage of 20 kV and a spot size of 5 μm. All elemental analyses utilized certified rare earth elements' standards for phosphates (REEP25-15 + FC, Astimex Standards Ltd., Toronto, ON, USA) and oxides (Standard block #489, Geller Microanalytical Laboratory). A microanalysis was completed by using Oxford Aztec Nanoanalysis software.

2.3. Sequential Extraction

To determine the solid fractions in which REEs were distributed, a seven-step sequential extraction modified from Lin et al. (2018) [20] and Ruttenberg (1992) [21] was applied. Through the seven-step process, the following fractions were sequentially extracted (Table 2): (1) water-soluble, using Milli-Q water (18.2 mΩ/cm, Millipore Corp. (Burlington, MA, USA)); (2) exchangeable, using 1 M ammonium sulfate; (3) acid soluble, using 1 M sodium acetate trihydrate [21]; (4) mildly reducible, using 0.1 M hydroxylamine

hydrochloride; (5) moderately reducible, using 0.2 M ammonium oxalate and 0.2 M oxalic acid; (6) strongly reducible, using 0.2 M ammonium oxalate, 0.2 M oxalic acid and 0.1 M ascorbic acid; (7) oxidizable, using a two-step acidified hydrogen peroxide digestion, followed by an ammonium acetate extraction; and the residual solids [20,24]. Sequential extractions of laterites and other geologic materials have been broadly used to establish geochemical associations between elements [18–20,24–26]. The labels associated with each step were defined in such a way as to represent the most likely targeted phase(s) in reference to previous studies conducted investigating similar relationships between materials, lixiviants, and extracted fractions.

Table 2. Seven-step sequential extraction conditions.

Step	Targeted Fraction	Hosting Phase Examples	Reagents	L:S Ratio (mL:g)	Temp (°C)	Duration (h)	pH
1	Water-Soluble		distilled water	20:1	25	24	5.8
2	Exchangeable	Clay	1 M ammonium sulfate	20:1	25	24	6
3	Acid Soluble	Carbonates and apatitic phases	1 M sodium-acetate trihydrate	25:1	25	24	4
4	Mildly Reducible	Amorphous Mn oxides	0.1 M hydroxylamine hydrochloride	20:1	25	0.5	3.5
5	Moderately Reducible	Crystalline Mn oxides, or amorphous Fe oxides	0.2 M ammonium oxalate + 0.2 M oxalic acid in dark	20:1	25	4 in dark	3
6	Strongly Reducible	Crystalline Fe oxides	0.2 M ammonium oxalate + 0.2 M oxalic acid + 0.1 M ascorbic acid	20:1	80	0.5	2.3
7	Oxidizable	Pyrite and/or organic matter	(1) acidified 30% H_2O_2	10:1	25/85	1 + 1	2
			(2) acidified 30% H_2O_2	10:1	85	1	2
			(3) 1M ammonium acetate wash	50:1	25	16	2
	Residual	Aluminosilicates	$LiBO_2$ Digestion	-	-	-	-

In preparation for the first extraction step, 2.5 g of each coal-related sample was ground to 100 mesh (<150 µm). During Steps 1–7 of the extraction, each solid sample was mixed with various extraction reagents (Table 2) and rotated in an end-over-end shaker (40 revolutions per minute) at room temperature. After each step, the samples were removed from the rotator and centrifuged for 20 min at a centrifugal force of 3000 relative centrifugal force (rcf). The solutions were decanted and filtered through nylon 0.45 µm filters and acidified and refrigerated before shipment to the National Energy Technology Laboratory (NETL) Pittsburgh Analytical Laboratory (PAL) for analysis. Trace, minor, and major elements were analyzed via inductively coupled plasma (ICP)–mass spectroscopy (MS) (Perkin Elmer Nexion 300D/350D) and optical emission spectroscopy (OES) (Perkin Elmer Optima DV7300/DV8300 2013) for bulk, sequential extraction, and residual samples. Each solid sample was rinsed twice to minimize any remaining reagent from the previous step being present on the solids. Both rinses occurred with the addition of 20 mL of MilliQ (18.2 mΩ/cm, Millipore Corp.) water, followed by 20 min of rotation on the end-over shaker at room temperature, and centrifugation for 20 min at 3000 rcf. Next, the solids were dried overnight at 60 °C, and their dry weight was recorded. Before the beginning of the next step approximately 0.5 g of dried solids were removed for analysis. The rest of the solid was weighed and noted as the starting weight for the next step. For Steps 1–6, weight loss was calculated to be below 5%. Weight loss was calculated to be 2%–13% for Step 7 due to static conditions in the laboratory. Cumulative percent weight

loss (weight loss due to approximately 0.5 g of solids being removed before the next step) was mathematically adjusted for and reflected in the reported extracted concentrations for each element. Duplicate extraction of the WV MKT underclay had a maximum relative error of 10%. The sequential extraction experiment had a mass balance of 98% for the WV MKT underclay sample, 101% for the WV MKT coarse coal refuse sample, 94% for the Central PA LKT underclay, and 108% for the Central PA MKT underclay sample. For the post-reaction liquid samples, the detection limit for REE on the ICP–MS was 3.5–8.4 ng/L. The residual solids underwent LiBO2 fusion (Walsh, 1980) at the NETL PAL, and then subsequently analyzed for trace, minor, and major elements via ICPMS and ICP–OES.

The grades and sources of chemicals used in this study follow. Ammonium sulfate (ACS grade), sodium acetate trihydrate (USP grade), ascorbic acid (ACS grade), ammonium oxalate (4% *w*/*v*) (ACS grade), ammonium acetate (ACS grade), oxalic acid (ACS grade), hydrogen peroxide (30% *w*/*v*) (ACS grade), and hydroxylamine hydrochloride (ACS grade) were purchased from Cole-Parmer Instrument Co., Vernon Hills, IL, USA.

3. Results and Discussion

3.1. Bulk Geochemical Composition and Mineralogy

Bulk values for REE ranged from 221 mg/kg to 728 mg/kg for the underclay samples (Table 3). All four coal-related samples had slightly elevated REE values as REE concentrations in the continental crust are typically around 169 mg/kg, REE concentrations in world coals are approximately 68.5 mg/kg, and REE concentrations in US coals are approximately 62.1 mg/kg [9,27]. The WV MKT underclay bulk sample, WV MKT coarse coal refuse bulk sample, and Central PA LKT underclay bulk sample had dry ash contents ranging from 92% to 96%. While a thermogravimetric analysis was not conducted on the Central PA MKT underclay bulk sample, the ash content is expected to be similar to the other samples (~90%). Bulk geochemical compositions of major elements and additional elements are shown in Table 4.

Table 3. Bulk chemistry of REEs in analyzed underclays. Units are reported in mg/kg.

	Sc	La	Ce	Pr	Nd	Sm	Eu	Gd	Tb	Dy	Y	Ho	Er	Tm	Yb	Lu	REE
WV MKT underclay	24	34	71	9	37	10	2.7	15	2.4	13	66	2.2	6	0.7	4	0.6	**297**
WV MKT coarse coal refuse	22	61	120	14	54	11	2.2	10	1.2	7	35	1.3	4	0.5	4	0.5	**345**
Central PA LKT underclay	17	37	69	8	30	6	1.2	6	0.9	6	32	1.1	4	0.5	3	0.5	**221**
Central PA MKT underclay	33	61	140	18	85	29	9.5	45	7.1	40	223	6.8	17	1.9	10	1.3	**728**

Table 4. Bulk chemistry of major and minor elements in underclays. Units are reported in wt.% or mg/kg based on concentration.

	Si	Al	Fe	Mn	Mg	Ca	K	P	Cr	Co	Ni	Cu	Zn
Unit	**Wt.%**	**Wt.%**	**Wt.%**	**mg/kg**	**mg/kg**	**Wt.%**	**Wt.%**	**mg/kg**	**mg/kg**	**mg/kg**	**mg/kg**	**mg/kg**	**mg/kg**
WV MKT underclay	26	11	4.4	194	5274	0.6	2.2	2097	132	65	130	89	203
WV MKT coarse coal refuse	28	12	1.7	95	5556	0.2	2.9	603	122	13	41	57	97
Central PA LKT underclay	33	10	1.0	40	3684	0.1	3.0	317	86	8	30	16	105
Central PA MKT underclay	21	9.0	2.7	194	6059	9.0	2.8	36,738	132	65	130	89	203

The XRD results (Figure 1) showed that the dominant mineral phases in all samples are quartz and clay minerals (kaolinite and illite). Of note, fluorapatite ($Ca_5(PO_4)_3F$) was detected in the Central PA and WV MKT underclay (Figure 1). The mineralogy was further analyzed by using electron microscopy. While the scope of this paper focuses on the sequential extraction of REEs in multiple targeted fractions and is supplemented by electron microscopy, additional microscopy efforts can be found in Montross et al. (2018) [16] and Yang et al. (2020) [5].

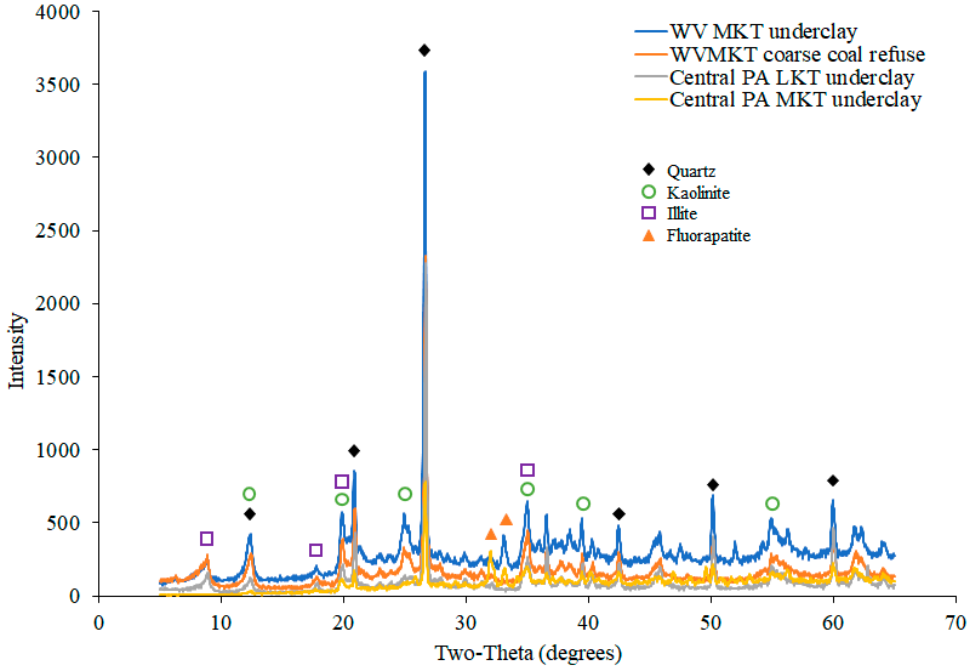

Figure 1. Semi-quantitative XRD data from the four coal-related samples.

Trace-mineral phases of interest in the WV MKT underclay were sphalerite end members ((Zn,Fe)S and ZnS), framboidal, euhedral and aggregated pyrite (FeS), and Fe-oxyhydroxides (Figure 2A). A Cu-Ni (with trace Fe) sulfur phase co-located with pyrite was determined by EPMA-WDS (Figure 2B). For REE-based minerals, there are fluorapatite and fibrous hydroxyapatite ($Ca_5(PO_4)_3OH$), as well as an altered aluminum phosphate known as crandallite (Ce, La-($CaAl_3(PO_4)(PO_3OH(OH)_6)$) within the sample (Figure 2C–E). This study also confirmed the rare presence of monazite ($(Ce,La,Nd)PO_4$) and xenotime (YPO_4) and the respective hydrated forms of rhabdophane ($(Ce,La)PO_4 \bullet H_2O$) and churchite ($YPO_4 \bullet 2H_2O$), as seen by Yang et al. (2020) [5]. In the WV MKT coarse coal refuse, the mineral phases of interest identified in electron microscopy were Ti-oxide, chromite ($FeCr_2O_4$), and chalcopyrite ($CuFeS_2$) embedded in crandallite (Supplementary Figure S2), as well as pyrite and monazite.

In the Central PA MKT underclay sample, there were bands of barite ($BaSO_4$) containing Co and Zn that were around 2.5 µm in length and 250 µm wide, pyrite (25 µm) framboids embedded in coal pockets and between clay bedding, and sphalerite (Supplementary Table S2). Nanoparticles with unidentifiable elemental composition (likely kaolinite, EPMA-WDS) were observed in the clay matrix (Figure 2F), as the fluorescence signal of the nanoparticles overlaps with the signal from the clay matrix. In addition to fluorapatite identified in XRD and microscopy, EPMA-WDS also identified (Ce, La)-hydroxyapatite (lacked fluorine, matrix correction based on stoichiometric oxygen). As with previous MKT underclay, trace amounts of monazite and xenotime were observed. On the other hand, while the Central PA LKT underclay sample was sourced from the same location as the Central PA MKT underclay sample, this underclay sample was unremarkable and comprised a quartz and clay matrix (kaolinite and illite) with detrital Ti-oxides. No secondary REE minerals were observed, and only 10–50 µm monazite and xenotime fragments were seen; the lack of REE hosting phases and subsequent limited REE extractability is discussed further in Sections 3.3 and 3.4.

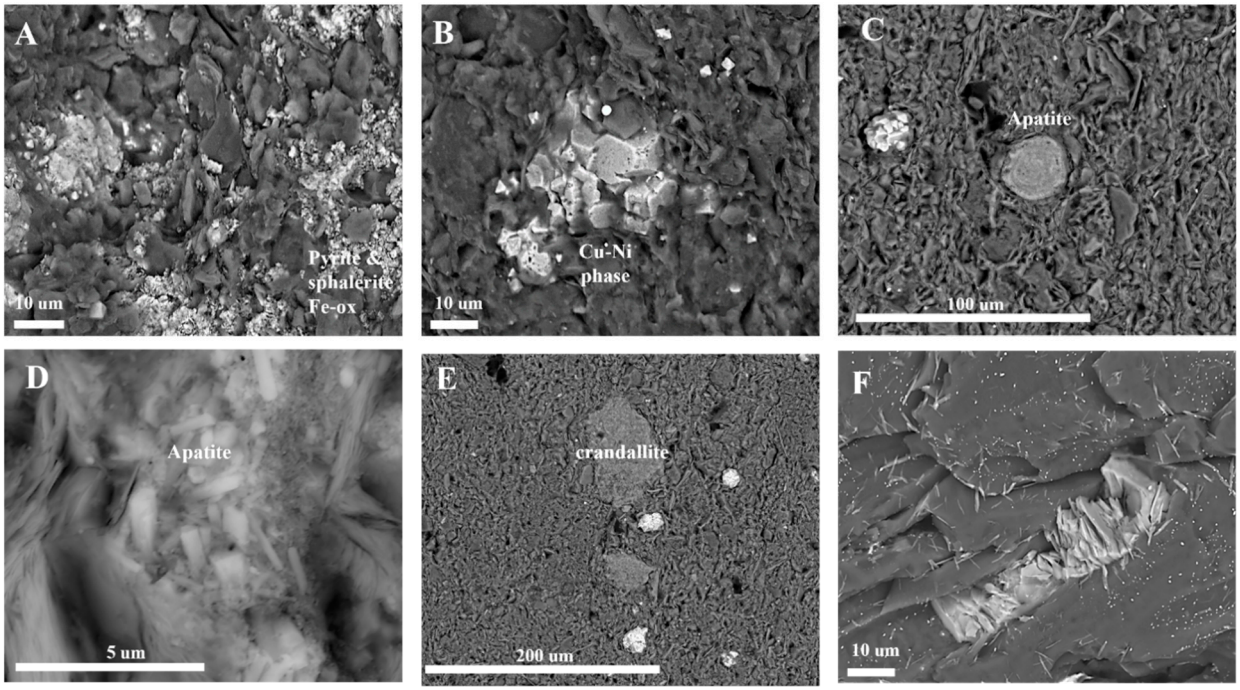

Figure 2. Electron images: (**A**) an agglomeration of pyrite, sphalerite, and Fe-oxyhydroxides within the clay matrix (WV MKT underclay); (**B**) Cu-Ni (+Fe) sulfate (WV MKT underclay); (**C**,**D**) crystalline and fibrous apatite (WV MKT underclay); (**E**) crandallite (WV MKT underclay); (**F**) clay matrix and nano-minerals (Central PA MKT underclay).

3.2. Critical Element Extractability

This study had a special focus on the easily extractable rare earth elements or critical minerals and characterized the associated solid fractions to inform future REE/CM recovery. Therefore, we report elements, such as REEs, recovered from all seven steps as extractable, whereas elements recovered from the residual solids post-seven-step extraction were reported as non-extractable.

The results from this study indicate that, for all four coal-related samples, less than 2% of Al, less than 5% of Si, and less than 6% of K were extractable, indicating that the majority of these elements remain in the residual phase, likely as aluminosilicates (e.g., quartz and illite). Additionally, the majority of Mg in all four coal-related samples is held in refractory phases with only 4%–8% of Mg extracted from the samples. The extracted concentrations of metals (As, Ba, Th, and U) were very low, indicating these elements as being held in immobile refractory silicate phases (non-extractable). The results from this study also suggest that Cr is locked in non-extractable phases such as aluminosilicates or chromite (Supplementary Figure S2), as only 2%–4% of Cr was extractable (Supplementary Table S2). Hot acid digestion is usually needed for the dissolution of chromite. In addition, H_2O_2 reactions can compete with the oxidation of Cr(III) and Fe(II) [25]. The minimal extracted Cr came out of the acid soluble and oxidizable fractions.

3.2.1. Fe and Mn

Distinguishing Mn-oxides from amorphous and crystalline Fe-oxyhydroxides is important for the targeted correlation of REE-bearing secondary minerals in source material. Many studies have examined sequential digestion methods in lateritic materials to evaluate the selectivity in these fractions [18,19]. Figure 3B shows that 29% of Mn in the WV MKT underclay and 22% of Mn in the Central PA MKT underclay were extracted as oxidizable phases, indicating the presence of Mn sulfides or Mn-associated organic matter phases. For both the WV MKT coarse coal refuse and the Central PA LKT underclay, more than 85% of the Mn was non-extractable (Figure 3B). For the Central PA LKT underclay, the

majority of extractable Mn came from the acid soluble phase possibly due to the dissolution of Mn carbonates (Figure 3B). Figure 3D shows that 19% of Fe in the WV MKT underclay and 9% of Fe in the Central PA MKT underclay were extracted as oxidizable phases. This, coupled with 4% of Fe in the WV MKT underclay being extracted from the acid soluble fraction with an observed drop in pH, indicates the presence of an Fe sulfide-based mineral such as precursor minerals for pyrite, mackinawite, or sphalerite [28]. Fe-sulfides phases (e.g., pyrite and sphalerite) are observed in the WV MKT underclay sample through SEM imaging (Figure 2A).

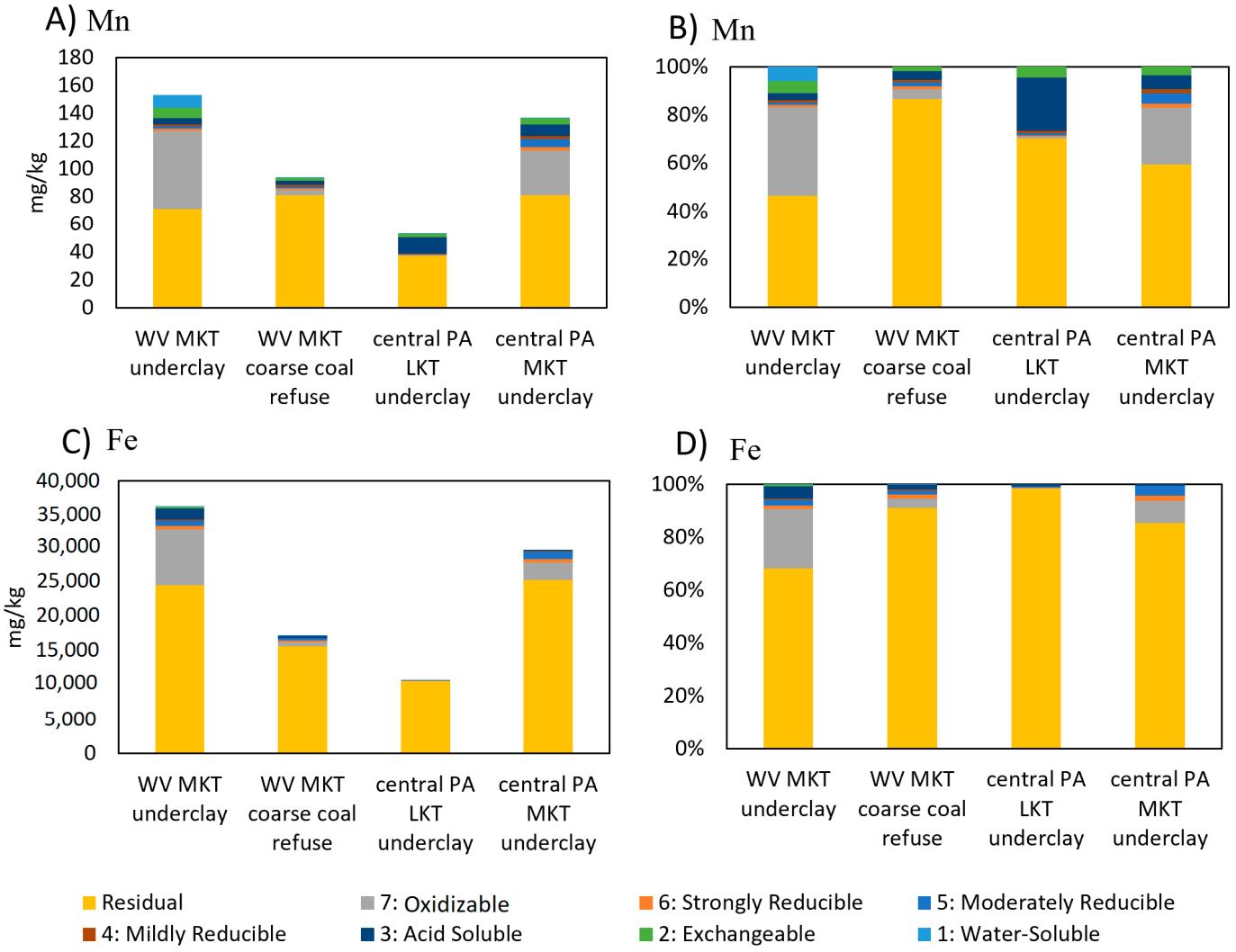

Figure 3. (**A**) Distribution of Mn from sequential extractions. (**B**) Plot of Mn distribution from sequential extractions normalized to percentage extraction. (**C**) Distribution of Fe from sequential extractions. (**D**) Plot of Fe distribution from sequential extractions normalized to percentage extraction.

3.2.2. Transition Metals: Co, Ni, Cu, and Zn

Sequential extraction results for Co, Ni, Cu, and Zn show early mobility within the initial steps targeting the exchangeable, oxidizable, water-soluble, and acid-soluble phases for all underclay samples, though the total mass should be noted as very low amounts (Figure 4). In these steps of the extraction, Co (44%–82%), Ni (20%–77%), Cu (42%–60%), and Zn (30%–68%) were extracted, with the WV MKT underclay showing the greatest mobility in these elements.

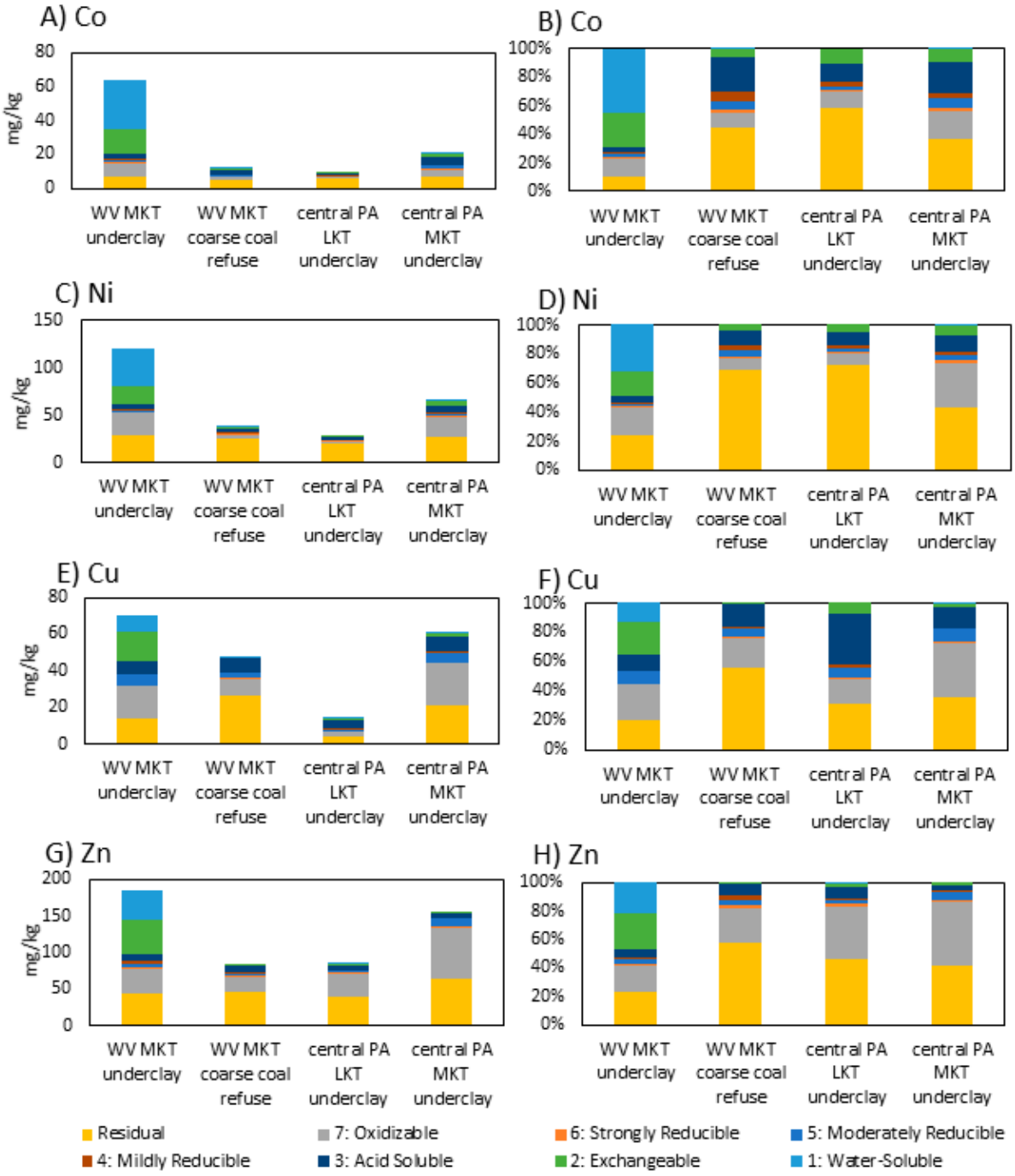

Figure 4. (**A**) Distribution of Co from sequential extractions. (**B**) Plot of Co distribution from sequential extractions normalized to percentage extraction. (**C**) Distribution of Ni from sequential extractions. (**D**) Plot of Ni distribution from sequential extractions normalized to percentage extraction. (**E**) Distribution of Cu from sequential extractions. (**F**) Plot of Cu distribution from sequential extractions normalized to percentage extraction. (**G**) Distribution of Zn from sequential extractions. (**H**) Plot of Co distribution from sequential extractions normalized to percentage extraction.

Co-extractability of these transition metals in the exchangeable and oxidizable fractions are of particular interest. Specifically, there seems to be a correlation between Co, Ni, Cu, and Zn with Mn and Fe mobility in the WV MKT underclay and the Central PA MKT underclay (Figures 3 and 4). A correlation between Cu and Fe mobility was also seen in the WV MKT coarse coal refuse. Chalcopyrite was observed in the WV MKT coarse coal underclay (Supplementary Figure S2), and both Cu and Fe were extracted from the

sample in the acid soluble and oxidizable fractions. This correlation was not seen in the Central PA LKT underclay. Based on the elemental extraction distribution, trace Fe/Mn mineral phases (e.g., sulfides such pyrite, chalcopyrite, and sphalerite; goethite; or other Fe or Mn-oxyhydroxides, as seen in Figure 2A,B) seem to host Co, Ni, Cu, and Zn.

3.2.3. Ca and P

Figure 5 shows that less than 5% of P was extracted from the seven extraction steps combined in the WV MKT coarse coal refuse and Central PA LKT underclay, whereas greater than 50% of Ca was extracted. Ca and P are both correlated with apatitic and crandallite phases, which are observed in these samples under XRD and SEM (Figures 1 and 2). However, the mobility of Ca and P in the sequential extraction steps differs significantly. In the two MKT underclay samples, approximately a quarter (28% for the WV sample and 26% for the Central PA sample) of P was extracted from the moderately reducible fraction (and to a lesser degree from the acid soluble fraction). In addition, some of P extracted could be associated with reducible Fe-oxide phases, as is commonly observed in marine sediments [29–32].

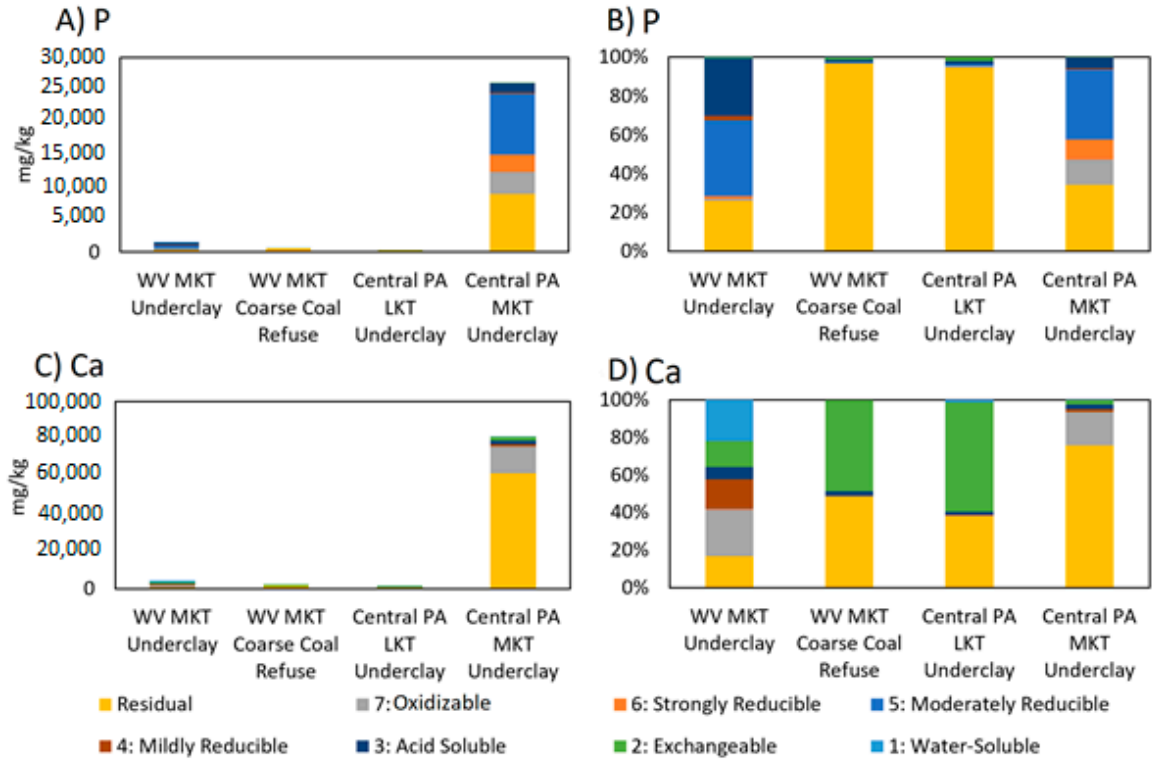

Figure 5. (**A**) Distribution of P from sequential extractions. (**B**) Plot of P distribution from sequential extractions normalized to percentage extraction. (**C**) Distribution of Ca from sequential extractions. (**D**) Plot of Ca distribution from sequential extractions normalized to percentage extraction.

Calcium was mainly extracted from the oxidizable phase in the MKT underclays (18% for WV and 16% for Central PA) (Figure 5D). Ca may also be associated with sulfate phases such as anhydrite (CaSO4), which is commonly found in coal seam environments [33]. In the WV MKT coarse coal refuse and Central PA LKT underclay, 47% and 61% of Ca, respectively, were extracted from the exchangeable fraction, showing that Ca in these samples were ion-adsorbed onto clay or mineral surfaces [5,20]. The remainder of the Ca is held in refractory minerals such as monazite, xenotime, or hydrated equivalents (Figure 5D).

3.3. REE Extractability

The majority of the REE exists in the residual phases for the studied MKT- and LKT-related samples. The breakdowns of the total REE extracted and critical elements of interest are included in Table 5.

Table 5. Total amount extracted (mg element extracted per kg underclay) and percentage (%) of REEs and elements of interest from the bulk compositions of coal-related samples.

	Total REE Extracted		Total Co Extracted		Total Ni Extracted		Total Cu Extracted		Total Zn Extracted		Total Al Extracted		Total Ca Extracted		Total Fe Extracted	
Sample	**mg/kg**	**%**	**mg/kg**	**%**	**mg/kg**	**%**	**mg/kg**	**%**	**mg/kg**	**%**	**mg/kg**	**%**	**mg/kg**	**%**	**mg/kg**	**%**
WV MKT Underclay	62	21	55	88	91	70	56	63	141	69	1780	2	3564	60	11,521	26
W V MKT Coarse Coal Refuse	6	2	7	51	12	29	21	37	35	36	1556	1	1186	50	1542	9
Central PA LKT Underclay	3	2	4	54	8	26	10	60	46	44	648	1	878	64	181	2
Central PA MKT Underclay	40	6	13	64	37	44	39	50	91	35	1585	2	19,655	22	4363	16

The total extractability of REEs for the WV MKT underclay was highest amongst the underclays studied at 21% (Table 5), with the majority found in the exchangeable and oxidizable fractions (Figure 6). For the WV MKT underclay, 8% of REE was extracted from the exchangeable fraction, and 8% of REE was extracted from the oxidizable fraction. For the WV MKT coarse coal refuse sample, the total REE extraction was <2%, indicating the majority of the REE bound in residual solids (Table 5). By contrast, easily soluble forms of apatite (e.g., carbonate fluorapatite and hydroxyapatite) might be expected to be mobilized under the acid soluble (Step 3) leach in the procedure. REEs are well-known to be associated with apatite phases in certain environmental conditions, and the REEs in these underclays were hypothesized to co-exist in an apatitic phase—the UCC normalized distribution patterns are reminiscent of P-bearing secondary minerals in sedimentary environments (Supplementary Figure S1) [21,34,35]. The REE, Ca, and P in the sample, however, were mobilized from different fractions, and this might imply that apatite was not an easily soluble REE host.

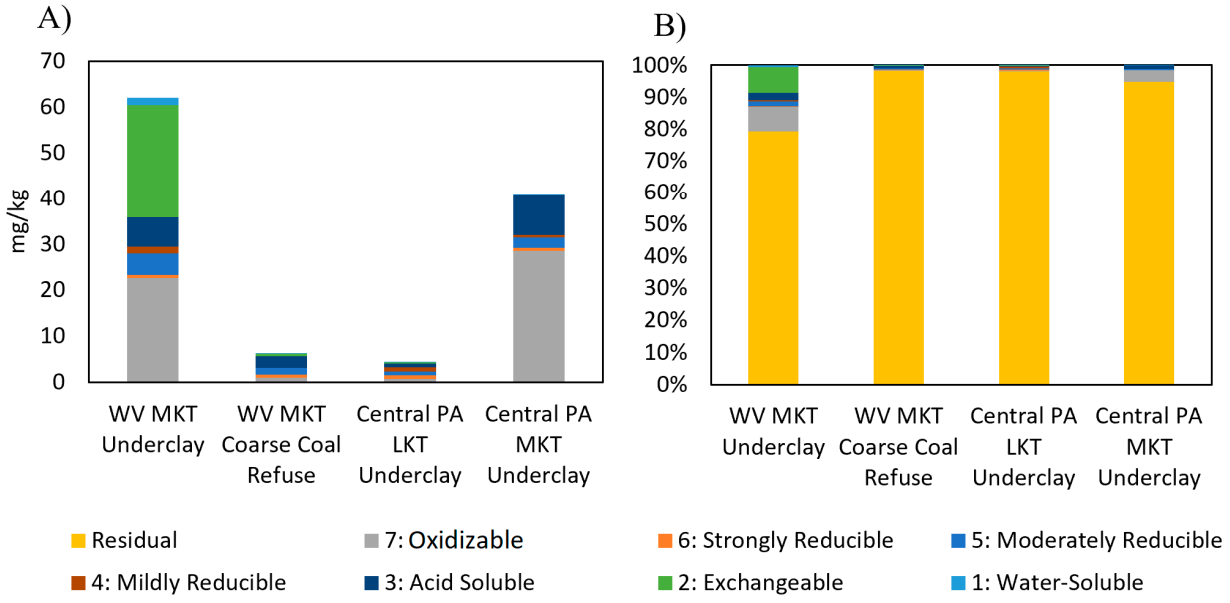

Figure 6. (**A**) Distribution of REE from sequential extractions excluding the residual fraction. (**B**) Plot of REE distribution from sequential extractions normalized to percentage extraction.

The Central PA LKT underclay had a total REE extraction of <2% (Table 5). The Central PA LKT underclay did not have REE extracted from the exchangeable fraction

from clays, thus indicating that no easily soluble REE-bearing clay minerals were present in the sample. The total extractability of REE for the Central PA MKT underclay was 6% (Table 5). However, the Central PA MKT underclay had the highest bulk REE concentration of the four samples, at 728 mg/kg, indicating some degree of enrichment above-average crustal values and average underclay values. A majority of REEs extracted were from the oxidizable fraction (28 mg/kg) and the acid soluble fraction (9 mg/kg), as seen in Figure 6A. While secondary mineral phases such as easily soluble apatitic phases (e.g., hydroxyapatite) discussed above were hypothesized to account for this accumulation, the disconnect of the REE from the extracted Ca and P, as well as the lack of REE mobility in sequential extraction steps, indicates that this may not be the case. Alternate explanations could lie in the morphology and specific mineralogy of any hypothesized apatite phases.

Refractory fluorapatite, for example, is more resistant to dissolution in mildly acidic conditions than carbonate fluorapatite [21,30]. REEs have previously been shown to be bound to secondary phosphate minerals in laterites [19]. While the data presented in this study suggest that the extractable REEs in the coal-related samples are not associated with more soluble forms of apatite minerals, the possibility remains that REEs could still be linked to more refractory morphologies held in the non-extractable residual fraction. A look into the relative distribution and fractionation patterns of the extracted REE may help elucidate this possibility.

3.4. REE Distribution

The distribution of extracted REEs for all four coal-related samples showed middle-REE and heavy-REE enrichment (Figure 7; Supplementary Figure S1), which can be compared to patterns observed in analogue environments. For example, Fe/Mn oxyhydroxides have been shown to be correlated with HREE enrichment in laterite horizons [26,36]. Sediments rich in Fe, as well as P, have also been shown to have MREE enrichment [37]. MREE enrichment has also been correlated in black shales to the authigenic formation of phosphates and carbonates during diagenetic processes [38]. Ore samples, specifically those with a high Fe content due to Fe oxyhydroxides (such as goethite), have been shown to have moderate MREE enrichment [37]. While qualitative MREE- and HREE-enriched patterns are not uniquely constrained to Fe oxide or P phases, the circumstantial evidence of high Fe and P, particularly in the WV MKT underclay and Central PA MKT underclay, and the identification of phases such as fluorapatite and crandallite from SEM, EPMA, and XRD analyses support these phases as the primary REE-accumulation mechanisms. Crandallite is known for hosting MREE, as well as being associated with Y, which has been identified in the two West Virginia samples (Figure 2E; Supplementary Figure S1). In the Central PA LKT underclay, the MREE/HREE could be attributed to the Mn-oxides or kaolinite or illite clays in which nearly 51% Al and 75% Mn were released during the acid-soluble phase. Al-phosphate minerals occurring within the cavities of kaolinite clays have been commonly observed in some coal samples enriched in REEs [39]. A majority of REEs (98%) in the Central PA LKT underclay, however, are bound to refractory apatite (e.g., refractory fluorapatite) phases and REE hosting phosphates.

The MREE and HREE enrichment in the extractable fractions is also of interest from an economic standpoint. Many MREEs and HREEs are in high demand across numerous sectors, and in a sellable form, such as a REE oxide, they have a higher net price than LREE oxides. Therefore, materials enriched in MREE and HREE can have a lower overall concentration while still being economically feasible to use as a feedstock for extraction. One parameter for evaluating the composition of a REE source comparatively to another is the outlook coefficient (Kout = (Nd + Eu + Tb + Dy + Er + Y/REEsum)/(Ce + Ho + Tm + Yb + Lu/REEsum)) [40]. The outlook coefficient is an index relating the ratio of the relative concentrations of critical REE (determined by market trends) to the relative concentrations of excess REEs [40]. For this index, higher coefficients indicate higher-grade REE-bearing feedstock. The WV MKT underclay had the highest outlook coefficient (5.6), followed by the Central PA MKT underclay (3.3), WV MKT coarse coal refuse (3.1), and the Central PA LKT underclay (3.1).

Therefore, of the four feedstocks, the WV MKT underclay has the highest-grade extractable REE of the four feedstocks (Figure 8).

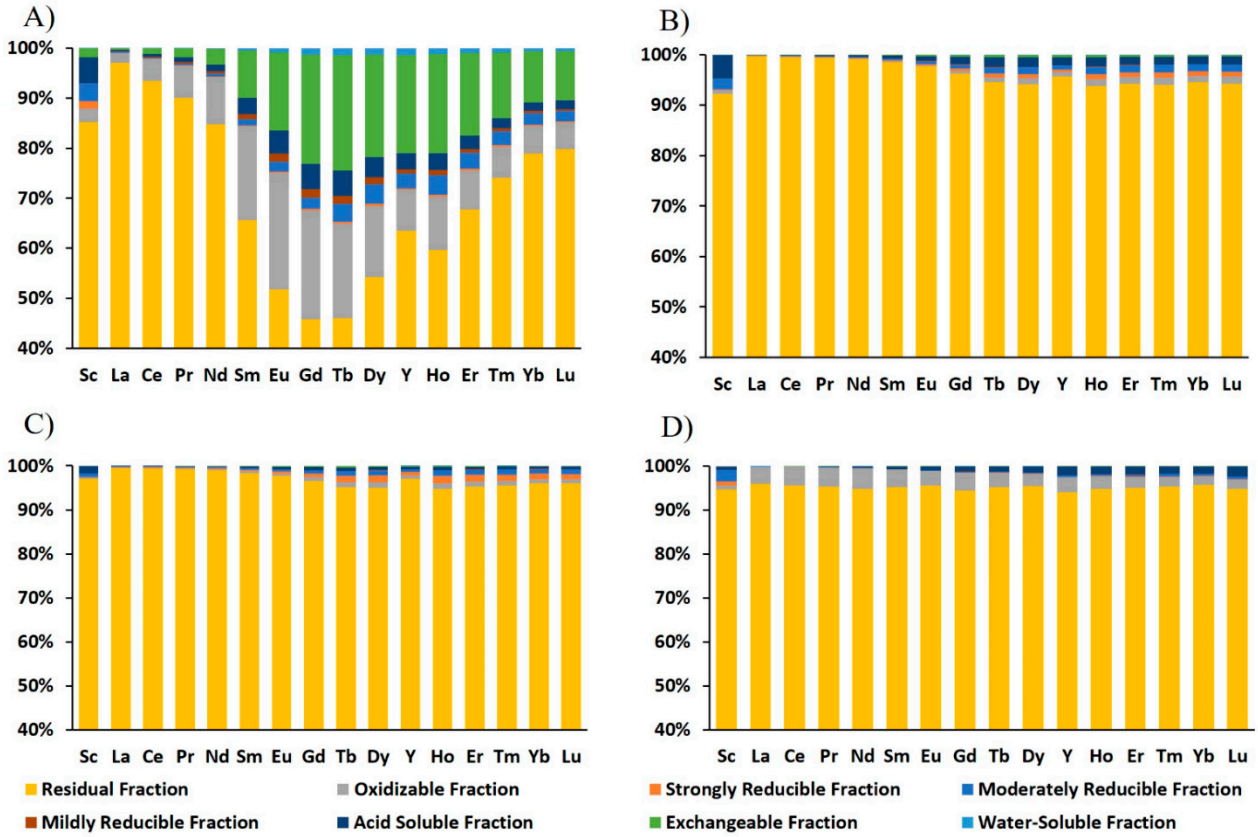

Figure 7. (**A**) Distribution of REE in WV MKT underclay normalized to percentage extraction. (**B**) Distribution of REE in WV MKT coarse coal refuse normalized to percentage extraction. (**C**) Distribution of REE in Central PA LKT underclay normalized to percentage extraction. (**D**) Distribution of REE in Central PA MKT underclay normalized to percentage extraction.

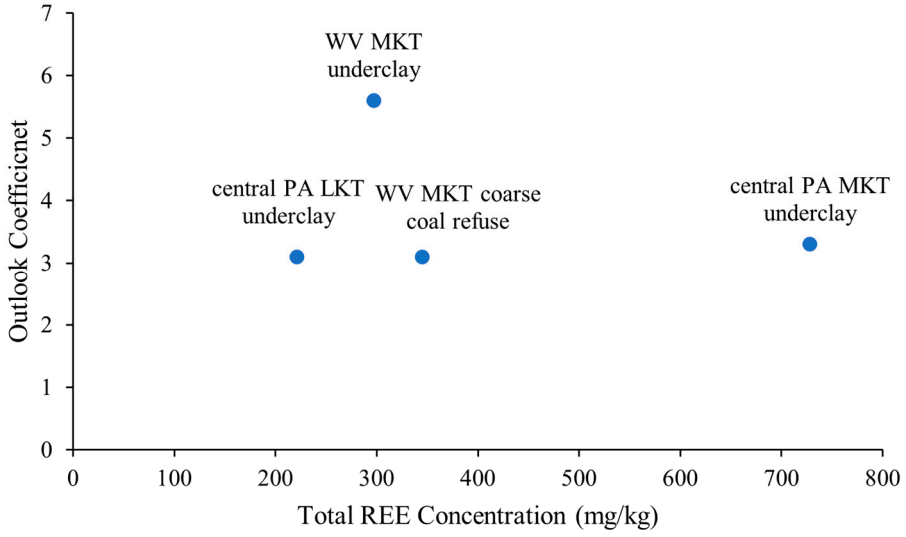

Figure 8. Outlook coefficient of each coal related sample plotted against the total REE concentration of each sample.

3.5. Heterogeneity between Coal Seams and Mining-Waste Streams

Variability is shown in the extractability of REE from coal-related feedstocks by the range of 2% to 21% of REE being extractable (Table 5; Figure 7). Variability in extractability of LREE, MREE, and HREE also occurred with MREE and HREE having higher extractability, as seen in Supplementary Figure S1A. Knowledge of the lattice-bound REEs expected to remain in residual solids can help determine which feedstocks will be economically feasible to extract REE from. Even within the same coal seam (i.e., Middle Kittanning) underclay, a high total REE concentration does not always equate to high extractability of REE. The Central PA MKT underclay sample contained a bulk REE concentration of 728 mg/kg, but only 40 mg/kg (6%) was able to be extracted. In contrast, the WV MKT underclay sample had a bulk REE concentration of less than half (297 mg/kg) of the Central PA MKT underclay sample but showed an extractability of 21% (62 mg/kg). The WV MKT underclay also had the highest outlook coefficient, showing that REE extracted from the sample had the highest relative concentration of critical REEs (Figure 8). Comparing underclay and coarse coal refuse from the same coal seam at the same sampling location, such as the WV MKT coal-related samples, it was determined that REE had a higher extractability from the underclay than the coarse coal refuse, even though their bulk REE concentrations were similar (Tables 3 and 5). While coal waste products such as coarse coal refuse may be acquired more easily than underclays, they may present a less ideal feedstock for REE extraction due to variability in total extraction shown.

The results from this study can be used to compare sequential extraction results from previous studies to determine if trends can be formed for the fractionation of mineral-bound REE in coal-related samples. In lateritic profiles that undergo extreme weathering, it was determined that REEs are bound to Fe-hydroxides and held in secondary REE-phosphate minerals [19]. This is comparable to the extractable REE found bound to Fe-hydroxides in the coal-related samples investigated in this study. However, any REE bound to secondary REE–phosphate minerals, such as apatitic phases hypothesized to hold extractable REE in the coal-related samples were held in the non-extractable fraction. REE-rich alkali basaltic laterite samples have also been shown to have the majority of REEs held in the non-extractable residual fraction after going through a six-step sequential extraction [41]. REE extraction from the alkali basaltic laterite samples showed minimal REE extracted from the ion-adsorbed/exchangeable fraction, the organic matter fraction, or the combined amorphous and crystalline Fe and Mn oxide fractions, and 5%–12% from the gibbsite/clays fraction [41]. The low extractability of REE from this study agrees with the results from the WV MKT coarse coal refuse, and the two Central PA samples. Initial mobilization of REE in the lateritic sequences from the above study or coal underclays from this study may be subsequently altered to more weather-resistant phases over time. A sequential extraction conducted on laterites from Western Australia also found the majority of REE to be non-extractable and held in weathering-resistant minerals in the residual fraction [42]. Second to the residual fraction, REEs were extracted from the water-soluble/adsorbed/exchangeable fraction in the Western Australian laterites, agreeing with REE extracted from the exchangeable fraction of the WV MKT underclay from this study [42]. The Fe (hydr)oxide fractions from the Western Australian laterites preferentially hosted MREE, which agrees with the MREE enrichment found in the coal-related samples from this study [42].

The results from this study can also be used to compare sequential extraction results from future studies to determine if trends can be formed for the fractionation of mineral bound REE in coal-related samples. Depending on the types of feedstocks examined in future work, certain steps, such as (mildly, moderately, or strongly) reducible steps, may be able to be combined to reduce experimental duration. Moreover, future experiments may benefit from limiting the reaction time for certain steps to partially constrain the release of gangue elements, such as Fe. Although this may reduce the amount of REE extracted from that step, the reduction in extracted REE may outweigh the benefit of reducing gangue elements, such as Fe, when thinking about costs associated with precipitation and

recovery of a salable product. The recovery of salable products can further be enhanced by the utilization of extractive methodology incorporating the knowledge obtained from sequential extractions regarding which mineral fractions contain both easily extractable REE and additional easily extractable critical minerals. The methodology of future extraction efforts targeting a specific sample type can be tailored to co-extract REEs and critical minerals in those easily extractable fractions. Creating methodology specifically targeting easily extractable fractions and excluding fractions containing less extractable and/or non-extractable fractions can assist with minimizing costs and utilization of resources. As seen in this study, high variability can occur between both underclay samples from the same coal seam, as well as between different coal-related samples from the same coal seam taken from different locations. While much useful information was gained from this experiment by comparing the same coal seam underclay from different locations, as well as coal underclay and coal waste from the same location, there are limitations to the extent of inference of the findings from this experiment due to only four total samples being analyzed. Therefore, these results should not be extrapolated to all Middle Kittanning coal by-products. However, this type of sequential extraction work used in tandem with other research on the same coal-related products can potentially help build a depositional model for REE in coal settings and which forms of REEs can be more extractable.

4. Conclusions

In this study, four samples associated with the Lower and Middle Kittanning coal seams from Pennsylvania and West Virginia were analyzed by using a seven-step sequential extraction. The total REE extractability ranged from 3 to 62 mg/kg, effectively from 2% to 21%. This variability was observed in the total REE concentration and was dependent on respective mineral fractions. The Central PA MKT underclay had the greatest bulk REE concentration (728 mg/kg), but REE extractability was an order of magnitude lower than that of the WV MKT underclay. The main phases of extractable REEs were found to be the exchangeable, oxidizable, and acid soluble fractions. In both the PA and WV MKT underclay samples, REE-bearing phosphate minerals may have been extracted from the moderately reducible phase. Additionally, REE-bearing Ca sulfide phases, such as anhydrite, may be extracted from the oxidizable phase of the PA and WV MKT underclay samples. The UCC normalized distribution patterns of the extracted REE are consistent with the patterns observed for Fe/Mn-oxyhydroxide phases and easily dissolvable calcium (alumino-)phosphate phases. In both the PA and WV MKT underclay samples, the mobility of Mn and Fe was found in the oxidizable fraction pointing to the possible association between mobility of REE at lower pH values. The remaining REEs are likely bound in more refractory phases, such as fluorapatite, monazite, or xenotime. Co-extraction of critical metals (Co, Ni, Cu, and Zn) was also observed to correlate with oxidation of sulfides and oxyhydroxide phases. REE extractability assists in the determination of future feedstocks and economic viability for salable REE.

Supplementary Materials: The following supporting information can be downloaded at https://www.mdpi.com/article/10.3390/min12111350/s1. Table S1: Bulk geochemistry of total REE extracted accumulated from Steps 1–7 of sequential extraction. Table S2: Bulk geochemistry of total extracted elements accumulated from Steps 1–7 of sequential extraction. Figure S1: Distribution of REE concentrations by elemental weight normalized to upper continental crust concentrations in four coal-related samples. Figure S2: SEM images from WV MKT coarse coal refuse and Central PA MKT underclay.

Author Contributions: Conceptualization, S.B., J.Y. and C.V.; methodology, S.B., J.Y., M.S. and C.V.; formal analysis, S.B., J.Y., M.S. and C.V.; investigation, S.B. and J.Y.; resources, S.B., J.Y., M.S. and C.V.; project administration, C.V. All authors have read and agreed to the published version of the manuscript.

Funding: This work was performed in support of U.S. Department of Energy's Fossil Energy and Carbon Management's Critical Mineral Sustainability Research Programs and executed through the National Energy Technology Laboratory (NETL) Research & Innovation Center's Critical Minerals Research Portfolio FWP-1022420.

Data Availability Statement: Not applicable.

Acknowledgments: We would like to thank Randal Thomas and Thomas Tarka for their support of the research as technology portfolio leads. Bill Garber, Phil Tinker, and Karen Johnson from the Pittsburgh Analytical Lab at NETL are thanked for their work in providing the sample analyses.

Conflicts of Interest: The authors declare no conflict of interest.

Disclaimer: This report was funded by the United States Department of Energy, National Energy Technology Laboratory, in part, through a site support contract. Neither the United States Government nor any agency thereof, nor any of their employees, nor the support contractor, nor any of their employees, makes any warranty, express or implied, or assumes any legal liability or responsibility for the accuracy, completeness, or usefulness of any information, apparatus, product, or process disclosed, or represents that its use would not infringe privately owned rights. Reference herein to any specific commercial product, process, or service by trade name, trademark, manufacturer, or otherwise does not necessarily constitute or imply its endorsement, recommendation, or favoring by the United States Government or any agency thereof. The views and opinions of authors expressed herein do not necessarily state or reflect those of the United States Government or any agency thereof.

References

1. Bauer, D.; Diamond, D.; Li, J.; Sandalow, D.; Telleen, P.; Wanner, B.U.S. *Department of Energy Critical Materials Strategy*; U.S. Department of Energy: Washington, DC, USA, 2010. [CrossRef]
2. Bauer, S.; Yang, J.; Verba, C. *Middle Kittanning Coal Waste and Underclay as an Alternative Rare Earth Elements Feedstock*; DOE.NETL-2021.2661; NETL Technical Report Series; U.S. Department of Energy, National Energy Technology Laboratory: Albany, OR, USA, 2021; p. 28. Available online: https://edx.netl.doe.gov/dataset/middle-kittanning-coal-waste-and-underclay-as-an-alternative-rare-earth-elements-feedstock (accessed on 27 July 2022). [CrossRef]
3. Balaram, V. Rare earth elements: A review of applications, occurrence, exploration, analysis, recycling, and environmental impact. *Geosci. Front.* **2019**, *10*, 1285–1303. [CrossRef]
4. Haxel, G.B.; Hedrick, J.B.; Orris, G.J.; Stauffer, P.H.; Hendley, J.W., II. *Rare Earth Elements: Critical Resources for High Technology*; USGS Fact Sheet 087-02; U.S. Department of the Interior: Washington, DC, USA; U.S. Geological Survey: Reston, VA, USA, 2002. [CrossRef]
5. Yang, J.; Montross, S.; Britton, J.; Stuckman, M.; Lopano, C.; Verba, C. Microanalytical approaches to Characterizing REE in appalachian basin underclays. *Minerals* **2020**, *10*, 546. [CrossRef]
6. Wang, Z.-Y.; Fan, H.-R.; Zhou, L.; Yang, K.-F.; She, H.-D. Carbonatite-related REE deposits: An overview. *Minerals* **2020**, *10*, 965. [CrossRef]
7. U.S. Geological Survey. *Mineral Commodity Summaries 2018*; U.S. Geological Survey: Reston, VA, USA, 2018; 200p. [CrossRef]
8. Cruse, A.M.; Lyons, T.W.; Kidder, D.L. Rare-earth element behaviour in phosphate and organic-rich host shales. In *Marine Authigenesis: From Global to Microbial*; Glenn, C.R., Prévot-Lucas, L., Lucas, J., Eds.; SEPM Special Publication: Tulsa, OK, USA, 2000; Volume 66, pp. 445–453. [CrossRef]
9. Seredin, V.V.; Dai, S. Coal deposits as potential alternative sources for lanthanides and yttrium. *Int. J. Coal. Geol.* **2012**, *94*, 67–93. [CrossRef]
10. Dushyanthaa, N.; Batapolaa, N.; Ilankoonb, I.M.S.K.; Rohithaa, S.; Premasiria, R.; Abeysinghea, B.; Ratnayakea, N.; Dissanayakea, K. The story of rare earth elements (REEs): Occurrences, global distribution, genesis, geology, mineralogy, and global production. *Ore Geol. Rev.* **2020**, *122*, 103521. [CrossRef]
11. U.S. Geological Survey. *Rare Earths Mineral Commodity Summaries/Minerals Yearbook, Various Issues*; 2021. Available online: https://www.usgs.gov/centers/nmic/rare-earths-statistics-and-information (accessed on 3 May 2021).
12. Fu, B.; Hower, J.C.; Zhang, W.; Luo, G.; Hu, H.; Yao, H. A review of rare earth elements and yttrium in coal ash: Content, modes of occurrences, combustion behavior, and extraction methods. *Prog. Energ. Combust.* **2022**, *88*, 100954. [CrossRef]
13. Appalachian Region Independent Power Producers Association (ARIPPA). Coal Refuse Whitepaper. 2018. Available online: https://arippa.org/wp-content/uploads/2018/12/ARIPPA-Coal-Refuse-Whitepaper-with-Photos-10_05_15.pdf (accessed on 3 February 2022).
14. Coal Refuse. Available online: https://www.rpmsolve.com/coal-refuse (accessed on 3 February 2022).
15. Montross, S.N.; Verba, C.A.; Chan, H.L.; Lopano, C. Advanced characterization of rare earth element minerals in coal utilization byproducts using multimodal image analysis. *Int. J. Coal. Geol.* **2018**, *195*, 362–372. [CrossRef]

16. Montross, S.N.; Yang, J.; Britton, J.; McKoy, M.; Verba, C. Leaching of rare earth elements from central appalachian coal seam underclays. *Minerals* **2020**, *10*, 577. [CrossRef]
17. Banfield, J.F.; Eggleton, R.A. Apatite replacement and rare earth mobilization, fractionation, and fixation during weathering. *Clay. Clay Miner.* **1989**, *37*, 2. [CrossRef]
18. Braun, J.-J.; Riotte, J.; Battacharya, S.; Violette, A.; Prunier, J.; Bouvier, V.; Candaudap, F.; Marechal, J.-C.; Ruiz, L.; Panda, S.R.; et al. REY-Th-U solute dynamics in the critical zone: Combined influence of chemical weathering, atmospheric deposit leaching, and vegetation cycling (mule hole watershed, south India). *Geochem. Geophy. Geosy.* **2017**, *18*, 4409–4425. [CrossRef]
19. Nasraoui, M.; Toulkeridis, T.; Clauer, N.; Bilal, E. Differentiated hydrothermal and meteoric altercations of the Lueshe carbonatite complex (Democratic Republic of Congo) identified by a REE study combined with a sequential acid-leaching experiment. *Chem. Geol.* **2000**, *165*, 109–132. [CrossRef]
20. Lin, R.; Stuckman, M.; Howard, B.H.; Bank, T.L.; Roth, E.A.; Macala, M.K.; Lopano, C.; Soong, Y.; Granite, E.J. Application of sequential extraction and hydrothermal treatment for characterization and enrichment of rare earth elements from coal fly ash. *Fuel* **2018**, *232*, 124–133. [CrossRef]
21. Ruttenberg, K.C. Development of a sequential extraction method for different forms of phosphorus in marine sediments. *Limnol. Oceanogr.* **1992**, *37*, 1460–1482. [CrossRef]
22. Zhang, R.; Li, Z.; Liu, X.; Wang, B.; Zhou, G.; Huang, X.; Lin, C.; Wang, A.; Brooks, M. Immobilization and bioavailability of heavy metals in greenhouse soils amended with rice straw-derived biochar. *Ecol. Eng.* **2017**, *98*, 183–188. [CrossRef]
23. Olaniran, A.O.; Balgobind, A.; Pillay, B. Bioavailability of heavy metals in soil: Impact on microbial biodegradation of organic compounds and possible improvement strategies. *Int. J. Mol. Sci.* **2013**, *14*, 10197–10228. [CrossRef]
24. Filgueiras, A.V.; Lavilla, I.; Bendicho, C. Chemical sequential extraction for metal partitioning in environmental solid samples. *J. Environ. Monitor.* **2002**, *4*, 823–857. [CrossRef]
25. Stuckman, M.Y.; Lopano, C.L.; Berry, S.M.; Hakala, J.A. Geochemical solid characterization of drill cuttings, core and drilling mud from Marcellus Shale Energy development. *Nat. Gas Sci. Eng.* **2019**, *68*, 102922. [CrossRef]
26. Denys, A.; Janots, E.; Auzende, A.-L.; Lanson, M.; Findling, N.; Trcera, N. Evaluation of selectivity of sequential extraction procedure applied to REE speciation in laterite. *Chem. Geol.* **2021**, *559*, 119954. [CrossRef]
27. Rudnick, R.; Gao, S. Composition of the Continental Crust. In *Treatise on Geochemistry*, 1st ed.; Rudnick, R., Ed.; Elsevier: Oxford, UK; Amsterdam, The Netherlands, 2003; Volume 3, pp. 1–64. [CrossRef]
28. Yu, C.; Drake, H.; Mathurin, F.A.; Åström, M.E. Cerium sequestration and accumulation in fractured crystalline bedrock: The role of Mn-Fe (hydr-)oxides and clay minerals. *Geochim. Cosmochim. Acta* **2017**, *199*, 370–389. [CrossRef]
29. Chen, J.; Algeo, T.J.; Zhao, L.; Cao, L.; Zhang, L.; Li, Y. Diagenetic uptake of rare earth elements by bioapatite, with an example from Lower Triassic conodonts of South China. *Earth Sci. Rev.* **2015**, *149*, 181–202. [CrossRef]
30. Anderson, L.D.; Delaney, M.L. Sequential extraction and analysis of phosphorus in marine sediments: Streamlining of the SEDEX procedure. *Limnol. Oceanogr.* **2000**, *45*, 509–515. [CrossRef]
31. Filippelli, G.M. Phosphate rock formation and marine phosphorus geochemistry: The deep time perspective. *Chemosphere* **2011**, *84*, 759–766. [CrossRef] [PubMed]
32. Kidder, D.L.; Eddy-Dilek, C.A. Rare-earth element variation in phosphate nodules from Midcontinent Pennsylvanian cyclothems. *J. Sediment. Res.* **1994**, *64*, 584–592. [CrossRef]
33. Liu, S.; Ma, W. Calcium-Bearing Minerals Transformation during Underground Coal Gasification. *Minerals* **2019**, *9*, 708. [CrossRef]
34. Zhang, L.; Algeo, T.J.; Cao, L.; Zhao, L.; Chen, Z.-Q.; Li, Z. Diagenetic uptake of rare earth elements by conodont apatite. *Palaeogeogr. Palaeocl.* **2016**, *458*, 176–197. [CrossRef]
35. Kidder, D.L.; Krishnaswamy, R.; Mapes, R.H. Elemental mobility in phosphatic shales during concretion growth and implications for provenance analysis. *Chem. Geol.* **2003**, *198*, 335–353. [CrossRef]
36. Liu, H.; Pourret, O.; Guo, H.; Bonhoure, J. Rare earth elements sorption to iron hydroxide: Model development and application to groundwater. *Appl. Geochem.* **2017**, *87*, 158–166. [CrossRef]
37. Yang, J.; Torres, M.; McManus, J.; Algeo, T.J.; Hakala, J.A.; Verba, C. Controls on rare earth element distributions in ancient organic-rich sedimentary sequences: Role of post-depositional diagenesis of phosphorus phases. *Chem. Geol.* **2017**, *466*, 533–544. [CrossRef]
38. Sokal, E.V.; Kokh, S.N.; Kozmenko, O.A.; Nekipelova, A.V.; Rudmin, M.; Khvorov, P.V.; Artemyev, D.A. Geochemistry and minerology of rare earth elements in high-phosphorus ooidal ironstones: A case study of the Kamysh-Burun deposit (Azov-Black Sea iron province). *Ore Geol. Rev.* **2020**, *127*, 103827. [CrossRef]
39. Li, B.; Zhuang, X.; Querol, X.; Moreno, N.; Córdoba, P.; Shangguan, Y.; Yang, L.; Li, J.; Zhang, F. Geological controls on the distribution of REY-Zr (Hf)-Nb (Ta) enrichment horizons in late Permian coals from the Qiandongbei Coalfield, Guizhou Province, SW China. *Int. J. Coal. Geol.* **2020**, *231*, 103604. [CrossRef]
40. Seredin, V.V. A New Method for Primary Evaluation of the Outlook for Rare Earth Element Ores. *Geol. Ore Depos.* **2010**, *52*, 428–433. [CrossRef]
41. Sanematsu, K.; Moriyama, T.; Sotouky, L.; Watanabe, Y. Mobility of rare earth elements in basalt-derived laterite at the Bolaven Plateau, southern Laos. *Resour. Geol.* **2011**, *61*, 140–158. [CrossRef]
42. Du, X.; Rate, A.; Gee, M. Particle size fractionation and chemical speciation of REE in a lateritic weathering profile in Western Australia. *Explore* **2012**, *157*, 1–14.